CHAPTER III

Methodology

3.1 Material Properties

There were two types of sand samples in this study. The first sand sample was taken from the eastern region of Thailand in Chonburi province. The grain particle slightly varies from rounded to sub-angular shape with low sphericity. The sand samples were then sieved to separate the grain particle to be in various dimensions. The sand particles resting on the sieve number 16 and 40 of U.S. standard size which has the opening equal to 1.18 and 0.425 mm., respectively would be selected as the test samples in the experiments. These uniformly graded sand samples will be called later by D16 and D40. The second sand sample was the commercial standard Silica test sand which has the well rounded shape of grain particle with high sphericity. This Silica test sand conforms to the ASTM C-778 #20 - 30. The mean size particle, d_{50}, is approximately 0.60 mm. The shape of grain particle of entire test sands can be shown in Fig. 3.1. To clearly observe the particle shape, the photo effect from the photo editing software was carried out. The results of that effect can be displayed in Fig. 3.2.

The basic engineering properties of sand samples shows in Table 3.1. It should be note that because of the low to medium sphericity and angular shape of each particle the mean size number (d_{50}) of D16 and D40 samples was the average value for the whole grain. The sample, after sieving, was washed out by clean water and the moisture was dried out in the electronic oven before the experiment.

3.2 Sample Preparation

Though, it is significantly understood that the sample preparation techniques for such a test of cohesionless materials can greatly influence the tested results. However, these types of preparation methods have their own advantages and disadvantages. For example, moist tamping method, though easy to perform, might

partially produce very loose to dense conditions of sample which consequently make a nonuniform specimen regarding of its entire density or particle size gradation. The air pluviation technique produces fairly uniform specimens depending upon the technique used. A higher drop height results in a higher energy of deposition and thus a denser soil specimen. Nevertheless, air pluviation of well-graded sand is not suitable because well-graded sand may become segregation when deposited by pluviation through air, especially if it has a considerable amount of fine contents. On the other hand, the influence of this segregation of well-sorted or uniformly graded sand is quite small.

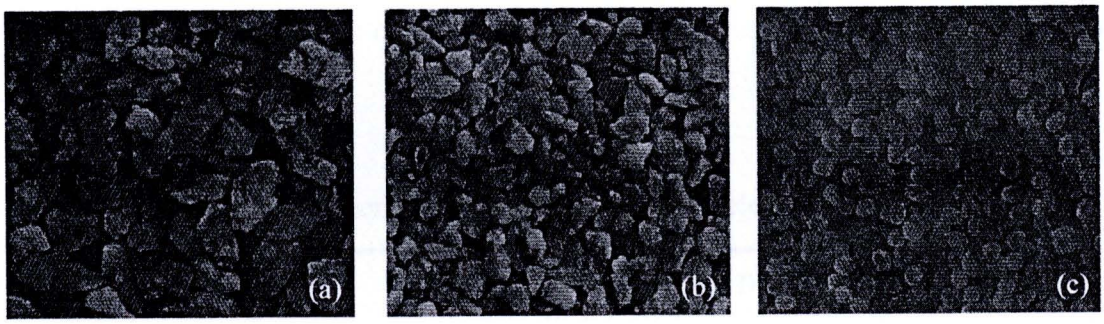

Figure 3-1 Shape of grain particle of (a) D16, (b) D40 and (c) Silica test sand.

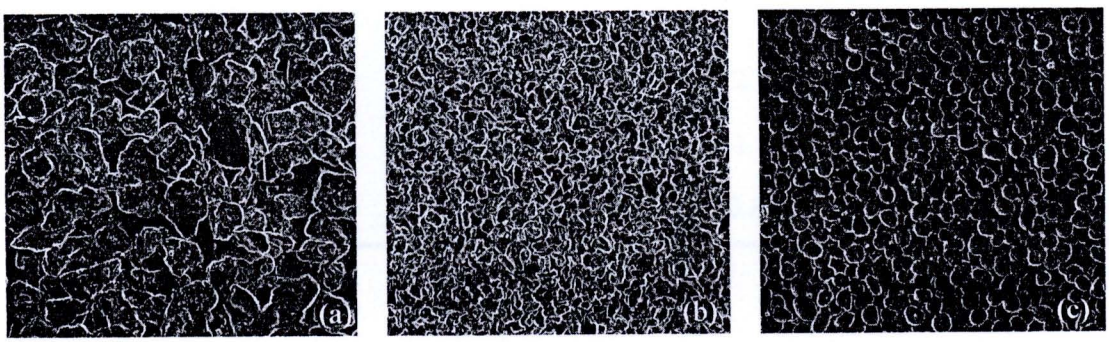

Figure 3-2 The photo effect of grain particles of (a) D16, (b) D40 and (c) Silica test sand.

In this study, the air pluviation technique was adopted because of the uniformity of the test sand particles and to prevent the separation between each layer in the composition procedure due to the difference in compaction energy of tamping method. Creating and maintaining a uniform sand rain during specimen reconstitution is really crucial because this is the main characteristic of pluviation and controls the uniformity of fabric and density. Five layers of test sand sample would be

consecutively dropped from a funnel with a constant height depending upon the required density of the specimen. Namely, the higher the drop of sand rains, the higher the density of the specimen. To prepare for very loose to loose conditions of the specimen, the nearly attached distance between the edge of the funnel and the reconstituted specimen, or null drop height, would be done. On the other hand, the medium to dense state would be performed by larger gap between the funnel and the top of the sand layer, i.e. about 5 - 8 cm. high. Moreover, to be certain that the desire relative density (D_r, %) would be acquired, the amount of the test sands would be calculated and weighted according to their basic engineering properties, e.g. minimum and maximum void ratio, specific gravity and dry density as in equations 3.1 and 3.2. The qualitative description of granular soil deposited into a specimen would follow Table 3.2.

Table 3.1 The basic engineering properties of sand samples

Basic property	**D16**	**D40**	**Silica sand**
Shape of grain particle	Low to medium sphericity with angular shape	Low to medium sphericity with angular shape	High sphericity with well rounded shape
Mean size particle, d_{50} (mm)	1.18	0.465	0.60
Specific gravity, G_s	2.69	2.72	2.65
Maximum void ratio, e_{max}	1.06	1.12	0.6
Minimum void ratio, e_{min}	0.713	0.808	0.459

$$e = \frac{G_s}{\rho_d} - 1 \tag{3.1}$$

where e is the actual void ratio, G_s is the specific gravity of soil, ρ_d is the dry density

$$D_r(\%) = \frac{e_{max} - e}{e_{max} - e_{min}} \times 100\% \tag{3.2}$$

where D_r is the percentage of relative density and e, e_{max} and e_{min} is the actual void ratio, maximum void ratio and minimum void ratio, respectively.

According to the literature, i.e. Desrues *et al.* (1996) and Desrues and Viggiani (2004), about the slenderness ratio of the sample, this study attempts to stay away from the unusual results form the triaxial tests. Desrues *et al.* (1996) could observe the complex patterns of shear band in a relatively short specimen, e.g. slenderness ratio = 1.0. However, in a long specimen, i.e. slenderness ratio = 1.94, the shear band exhibits itself in a form of single unique plane. They finally reported that the slenderness ratio greatly influences the strain localization in sand. Therefore, to avoid the complex pattern of shear band as well as some undesirable outcomes, the dimension of the specimen would be maintained to have the appropriate slenderness ratio; about 2.0. The typical height and width varied between 11.20 - 11.80 cm and 4.80 - 4.95 cm, respectively. The slenderness ratio, *H/D*, is therefore approximately 2.30 - 2.45.

Table 3.2 Qualitative description of granular soil deposits

Relative density (D_r, %)	**Description of soil deposits**
0 - 15	Very loose
15 - 50	Loose
50 - 70	Medium
70 - 85	Dense
85 - 100	Very dense

It should also be noted that to reduce the friction effect between the specimen and the top / bottom end platens (filter paper), the silicon grease should be lubricated on the surface of both ends every time prior to the test.

3.3 Bender Element

Depending on polarization, there are two types of bender element: series-type (x-poled) and parallel-type (y-poled). From the energy point of view, there is no difference between x-poled and y-poled bender elements. The bender elements used in this study were both series- and parallel- types. The parallel-type bender element

was used as a source and the series-type bender element as a receiver because the parallel-type connection gives twice the displacement of the series-type connection (Lee and Santamarina, 2005). One of the most important aspects associated with the use of bender elements is the waterproofing of the elements. Since piezo-ceramics are high impedance devices that may short circuit when contact with moisture. Therefore, the waterproof material, i.e. epoxy glue, was entirely coated to all surface of bender elements. The shielded wires were then connected with the bender element according to its type of connection. The shielded wires were used in order to minimize noise interfering with the signal.

The bender elements were then fixed into the slot of the top and bottom pedestals of the conventional triaxial apparatus by resin hardener. The protrusion of the bender element was 9.65 mm. for top cap and 9.80 mm. for top bottom cap. The schematic view of the installation of bender element in the pedestals can be shown in Figure 3.3.

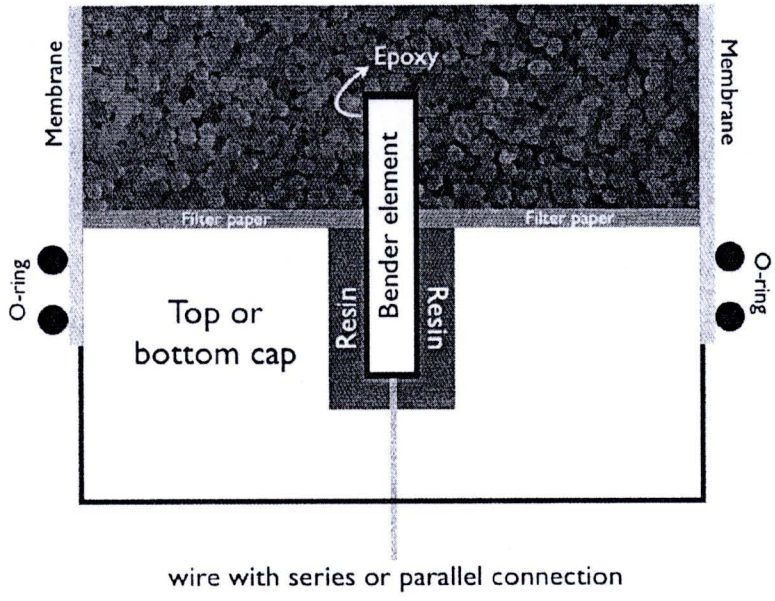

Figure 3.3 The installation of parallel- or series-type of bender element in the top / bottom cap of the triaxial apparatus

3.4 Digital Image Analysis (DIA)

Nowadays, DIA techniques are very powerful for gathering information to study the fabric and deformation of granular materials in geotechnical engineering. In the study of localization and shear band in soil sample, one of the simple and extensively used methods is the visual observation from the deformation profiles of the sample surface, i.e. membrane surface. Though, this technique cannot be used for the microscopic study of the deformation and failure mechanisms but can use to some extent to measure the thickness and inclination angle of the shear band. The series of square grid or dot will be imprinted on the membrane surface and the images will be captured by high resolution digital camera or video camera.

In this study, the surface of membrane would be lined by a waterproof and permanent pen. The dimension of these blue square grids is 5 x 5 mm. Figure 3.4 shows the square grid pattern of the specimens. The high resolution image, 2848 x 2136 pixels, was acquired by Fuji Finepix S6500fd digital camera. A series of image captures would be performed before, during and after the compression test. The digital camera was mounted on a camera stand in the fixed position for the entire process. It should be note that during the triaxial compression test, the images of the sample would be taken in every 0.5 mm. of axial deformation. When the axial strain is approximately more than 10% or when the shear band is obviously developed, the last snapshot of the failure specimen would be performed. However, because of the unpredictable zone of the localization inside the failure sample in the triaxial test, the suitable plane of the failure sample would be selected for a final shot of the image.

3.5 Triaxial Compression Test by Vacuum Technique

Due to the necessity of shear band observation by DIA, the conventional triaxial compression test by applying water pressure as a sample confinement will interfere the snapshot of specimen pictures during the test. Therefore, the triaxial compression test by vacuum technique would be adopted in all tests. The confining pressure was obtained by applying an internal vacuum inside the specimen, without a confining cell. However, the vacuum capacity is very limit, i.e. about 90 kPa.

Therefore, in this research, the maximum isotropic confining pressure would be around 80 kPa. Before filling the test sands into the mold for constituting the specimen, the partially vacuum pressure, e.g. 8 - 10 kPa, was applied to help smoothing the membrane attaching inside mold surface and to support the constituted specimen after disassembling of the mold. Any of the test procedures are similar to the conventional triaxial test. All of triaxial compression tests will be in dry condition. No pore water pressure and volume change would be measured and recorded.

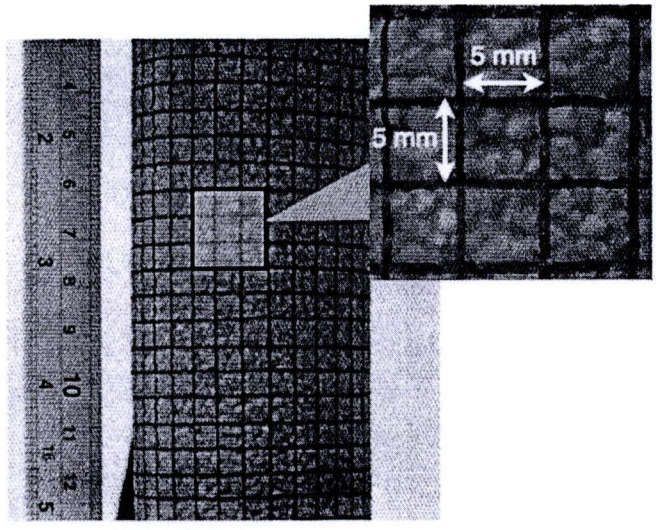

Figure 3.4 The printed square grid on the rubber membrane surface of the specimens

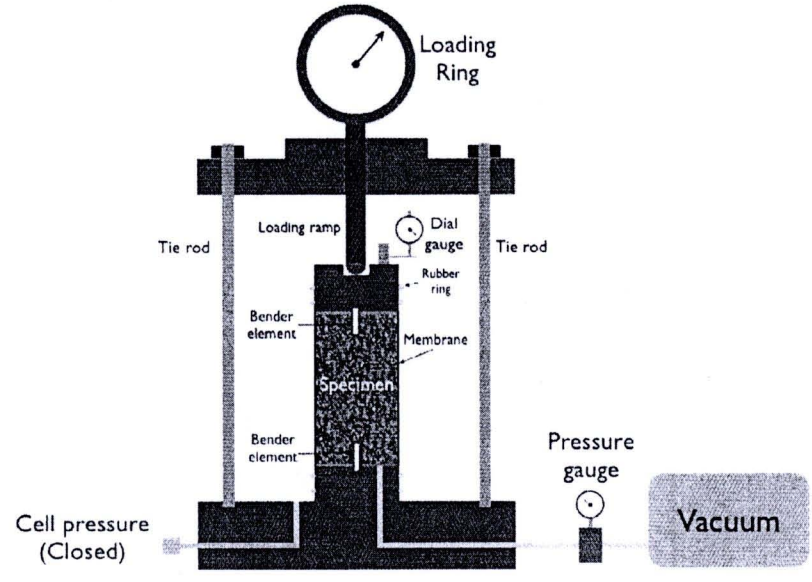

Figure 3.5 The schematic view of triaxial testing by vacuum technique

3.6 Experimental Works

The major apparatuses required in this research are;

1) Conventional triaxial compression apparatus modified to accommodate the bender elements

2) Bender elements installed in the top cap and pedestal of triaxial device

3) Oscilloscope and signal data acquisition software

4) Function generator (square wave trigger)

5) High resolution digital camera and stand

6) Computer

The schematic view of the bender element test setup incorporated in a triaxial cell apparatus can be shown in Figure 3.6.

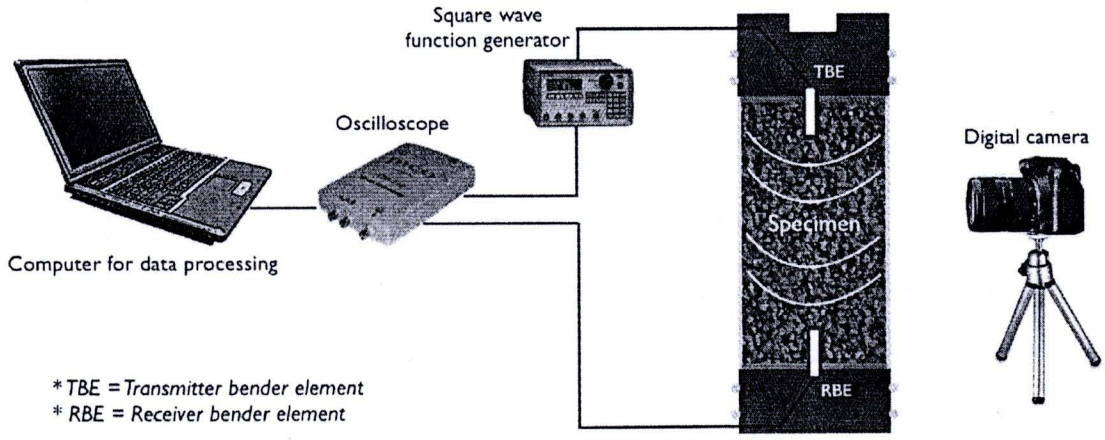

Figure 3.6 The schematic view of the bender element test setup incorporated in a triaxial cell apparatus

The commercial digital oscilloscope model, ADC-212, and wave data acquisition software by Pico Technology Limited was employed in the experiments. Because of many electrical devices e.g. personal computer and oscilloscope, used in the testing system, the ground of every apparatus was connected directly to the ground of the computer to minimize interference. The square wave function generator was connected to the oscilloscope and the transmitter bender element. The oscilloscope would then analyze the signal of both transmitter and receiver signals

and transferred theses signals to the data acquisition software in the computer for further signal processing. These data would be stored for future calculation and numerical analysis of V_s traveling inside the specimen. The figure of the transmitter square wave and received wave from the software shows in Fig 3.7.

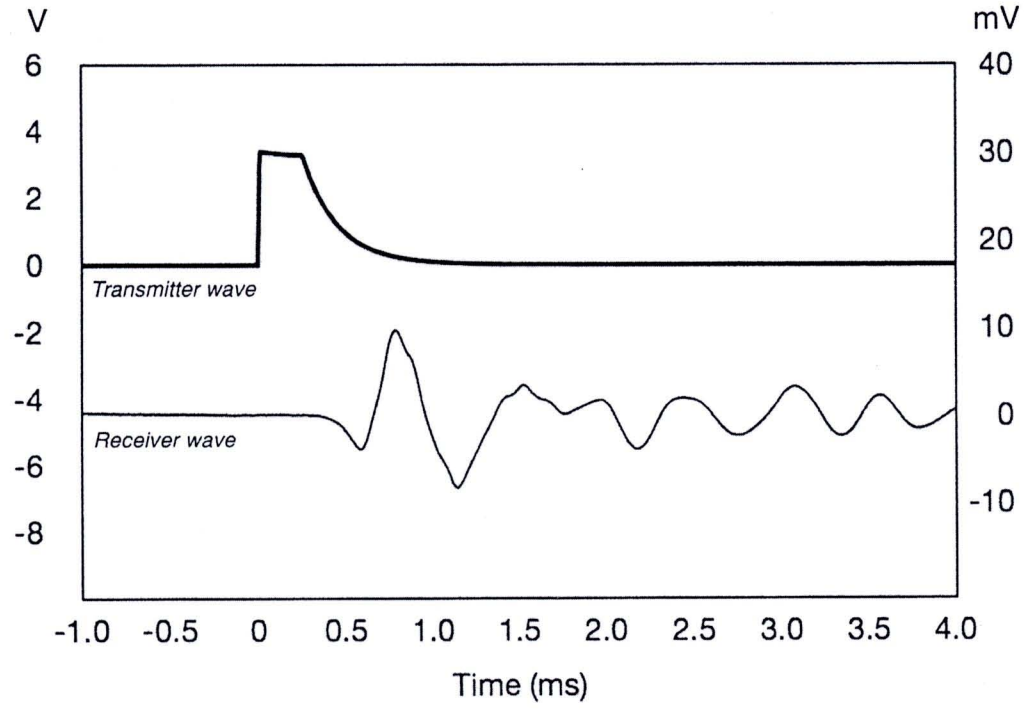

Figure 3.7 The graphical display of typical transmitter and receiver wave from oscilloscope processing

Before starting any triaxial compression tests, the entire system would be calibrated to correct some existing errors of the travel time and shear wave measurement as well as to minimize the interference from the noise of the surrounding apparatuses. It was found that the received signal was alway intervened by the nearby electrical devices. The appropriate grounding of all devices should be carefully performed.

The triaxial tests would be carried out with the vacuum confinement of 25, 50 and 80 kPa. Three types of test sand, i.e. D16, D40 and silica were reconstituted into various conditions, e.g. very loose, loose, medium and dense state. It should be note that the cases of very loose and medium condition were tested only for silica sand. The measurement of shear wave travel time and the snapshot of specimen before,

during and after testing would be performed and saved into the computer for further analyses. It should be noted that during the triaxial compression test, the loading machine would be momentarily halted, i.e 1-2 seconds, in every 0.5 mm of axial deformation while the specimen image was being captured by digital camera at its surface membrane. Although, this action might somewhat influence stress-strain relationship of the test but can considerably minimize the interference signal and vibration from the electrical motor machine.

The data of axial loading from proving ring and the axial deformation from dial gauge would also be recored to observe the stress-strain relation of the sample. This stress-strain relation can explain to some extent the initiation of the shear band or localization inside the sample under triaxial test.

Summary of testing and specimen conditions can be shown in Table 3.3 and the schematic chart of testing procedures can be shown in Figure 3.8

3.7 Calculation of Travel Time and Shear Wave Velocity

To calculate the shear wave velocity, V_s, traveling between transmitter and receiver bender elements, a conventional equation as in 3.3 is widely used among the researchers.

$$V_s = \frac{L_{tr}}{t} \tag{3.3}$$

where L_{tr} is the distance between tip of transmitter to receiver bender element and t is the traveling time (time-of-flight) of shear wave from transmitter to receiver bender element. Though this equation can easily calculate the V_s propagating throughout the soil specimen but the determination of t is still ambiguous. There are many controversial methods, e.g. first deflection, first bump maximum, zero crossing after first bump, and major first peak, to determine the first arrival time of propagated shear wave inside soil sample by using the bender elements.

Viggiani and Atkinson (1995) concluded from the numerical analyses that the travel time of the signals from bender elements tests on a reconstituted boulder clay

sample should not be taken as the time corresponding to the first deflection of the received signal. The travel time corresponding to the first inversion of the received signal is more accurate.

Table 3.3 All testing conditions and specimen properties of this study

Sand	Confining pressure (kPa)	Relative density		Specimen dimension			Image capture
				H (cm)	D^* (cm)	Slenderness ratio (H/D)	
D16	25	43.75%	Loose	11.49	4.79	2.39	Yes
		80.98%	Dense	11.80	4.81	2.45	Yes
	50	47.26%	Loose	11.22	4.82	2.32	Yes
		73.09%	Dense	11.67	4.86	2.40	Yes
	80	38.78%	Loose	11.22	4.87	2.30	Yes
		75.66%	Dense	11.54	4.87	2.37	Yes
D40	25	28.65%	Loose	11.27	4.81	2.34	Yes
		79.32%	Dense	11.35	4.85	2.34	Yes
	50	39.85%	Loose	11.21	4.79	2.34	Yes
		81.60%	Dense	11.45	4.82	2.37	Yes
	80	32.48%	Loose	11.27	4.95	2.27	Yes
		81.58%	Dense	11.67	4.78	2.44	Yes
Silica	25	13.58%	Very loose	11.51	4.91	2.34	Yes
		56.83%	Medium	11.50	4.90	2.35	Yes
	50	38.99%	Loose	11.44	4.82	2.37	Yes
		77.09%	Dense	11.19	4.87	2.29	Yes
	80	22.77%	Loose	11.49	4.87	2.35	Yes
		60.66%	Medium	11.44	4.89	2.33	Yes

* $D = \frac{D_{top} + 2D_{middle} + D_{bottom}}{4}$

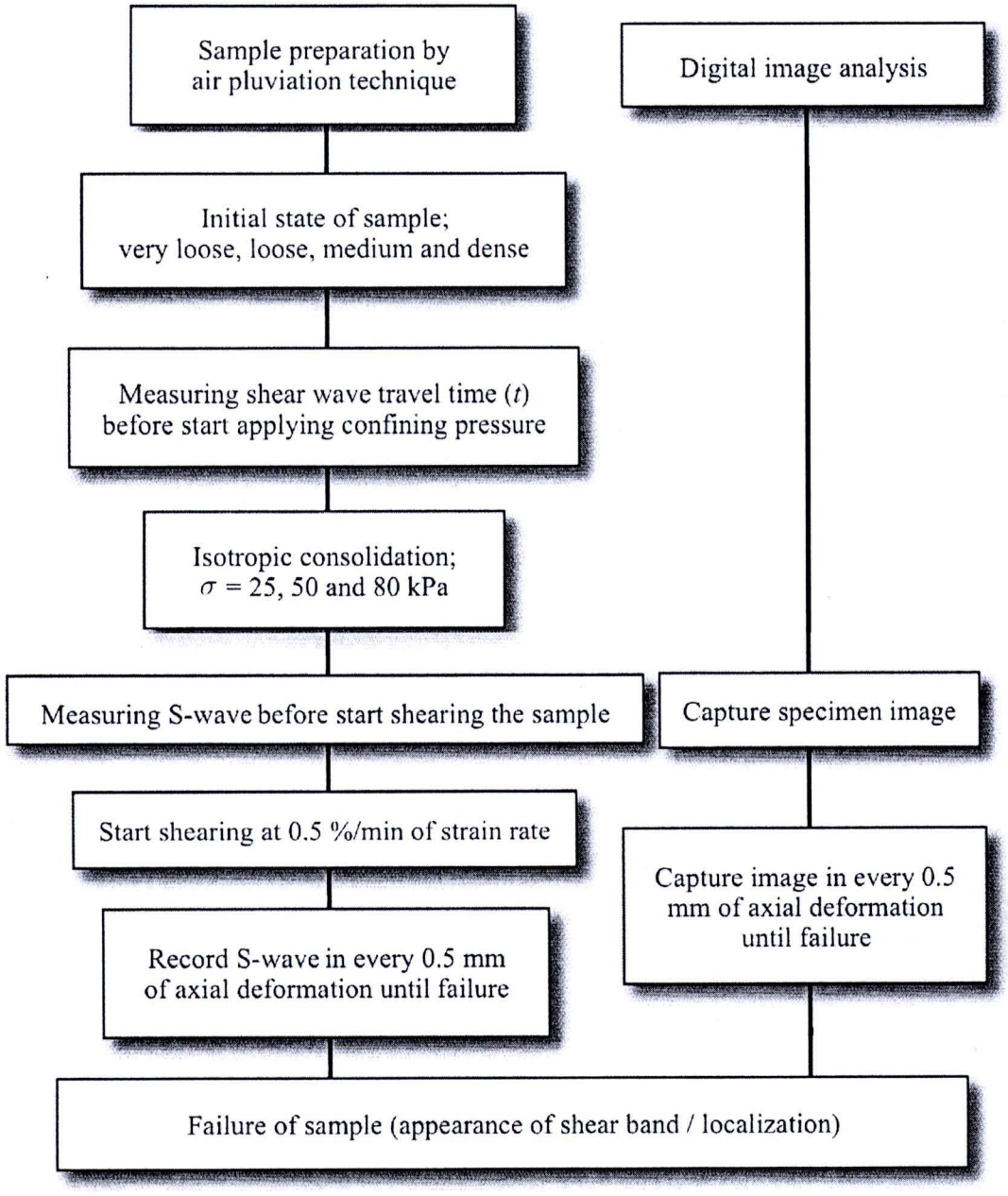

Figure 3.8 The schematic chart of all testing procedures

Leong *et al.* (2005) compared the travel time of a mudstone residual soil specimen at a confining pressure of 800 kPa. between the ultrasonic test and conventional bender element tests. The travel times for both the bender element test and the ultrasonic test are the same only if the first deflection of the receiver signal was used for the bender element test.

Lee and Santamarina (2005) described various techniques to determine the first arrival time between source and receiver bender elements as in Figure 3.9. They

also demonstrated that suggested criteria and recommendations to measure this first arrival time vary depending installation, application and input signal.

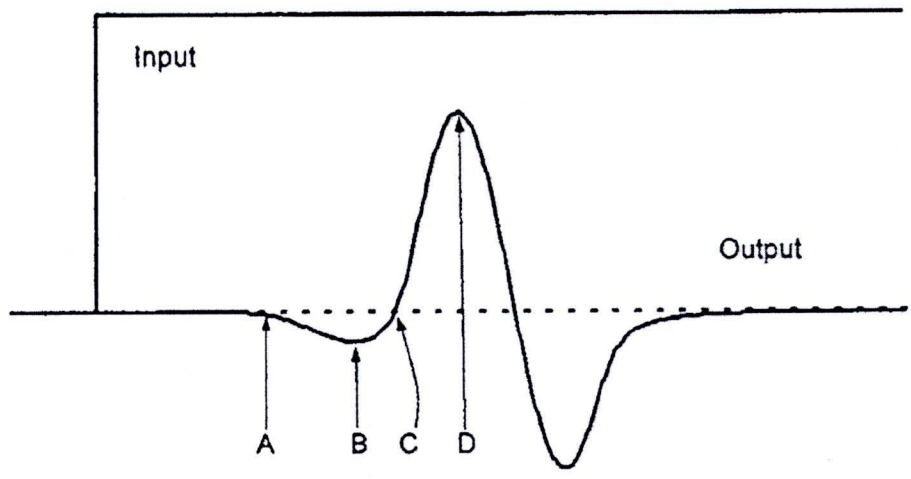

Figure 3.9 Typical *S-wave* signal within near field A) first deflection, B) first bump maximum, C) zero after first bump, and D) major first peak (Lee and Santamarina, 2005)

Therefore, it can be discerned from those previous reports that the method to choose the first arrival time of received signal to calculate for V_s slightly varies among the past experiments. There are a number of reasons which make this traveling time calculation complicated, for example, the interference between *P-waves* and *S-waves* (shear wave) at the first part of the received signal, the excitation frequency of the input signal as well as the near field effect. The *P-waves* which are also generated from the transmitter bender element generally reflect from the cell wall and always arrive earlier than the shear wave. Therefore, these reflecting *P-waves* will mainly disguise the interpretation of the first arrival time of the shear wave. The near field effect is usually occurred in short specimen and when L_{tr}/λ is less than 2. This effect will decrease as L_{tr}/λ increases (Sanchez-Salinero *et al.*, 1986 and Brignoli *et al.*, 1996) where λ is the wavelength of the shear wave.

In this research, because of a broad range of shear wave velocity determination in one test, i.e. from zero strain to failure, the variation of stress state and void ratio during shear will certainly affect the shear wave propagation characteristic. At any certain strain level the near field effect as well as the reflecting

P-wave may dominate or diminish depending on that current state of the soil. As a result, the manual visualization and interpretation of captured high-resolution image of signal from oscilloscope processing to select the appropriate first point of shear wave arrival would be adopted to calculate the shear wave velocity propagating throughout the specimen. The influences of *P-Wave* and near field effect would be carefully accounted in the result interpretation. Figure 3.10 shows the interpretation practice to point out the first arrival time of shear wave transmitted from the source to the receiver bender element justified for the near field effect and reflecting *P-waves*. It can be seen that the position of line Y is approximately the same as point B (first bump maximum) in Figure 3.9 where line X is the starting time of generated signal of transmitter bender element. The traveling time, *t*, will be the different between line X and Y. Figure 3.11 shows the effect of the near field and reflecting *P-waves* of the receiver signal.

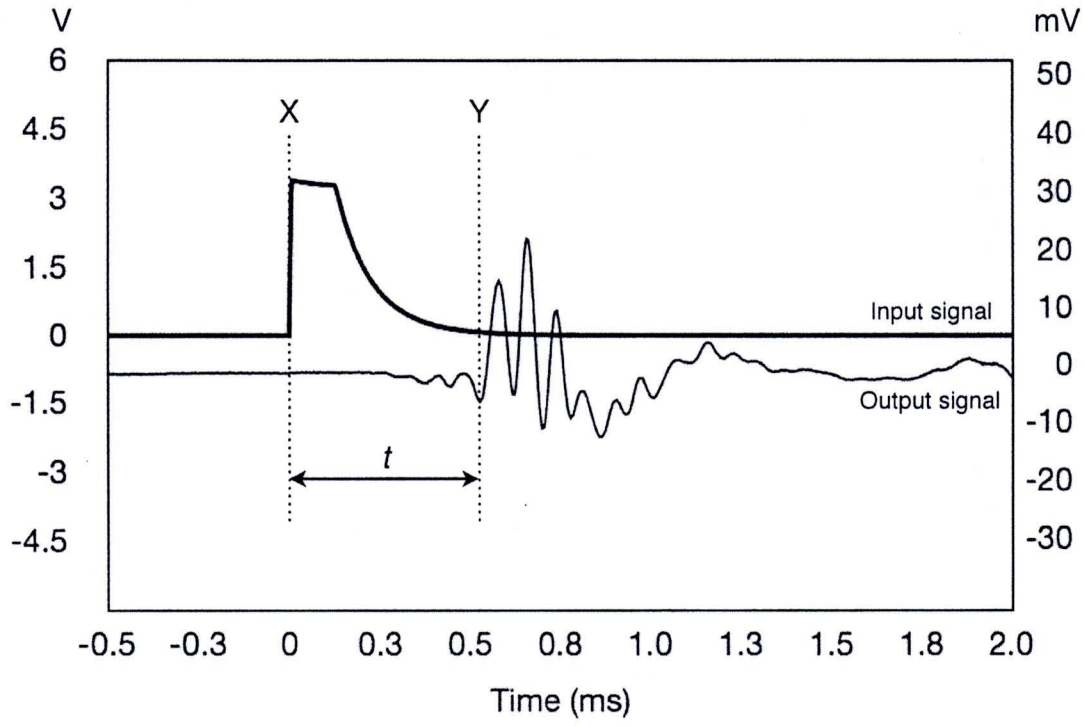

Figure 3.10 The interpretation method to point out the first arrival time of shear wave justified for the near field effect and reflecting *P-waves*.

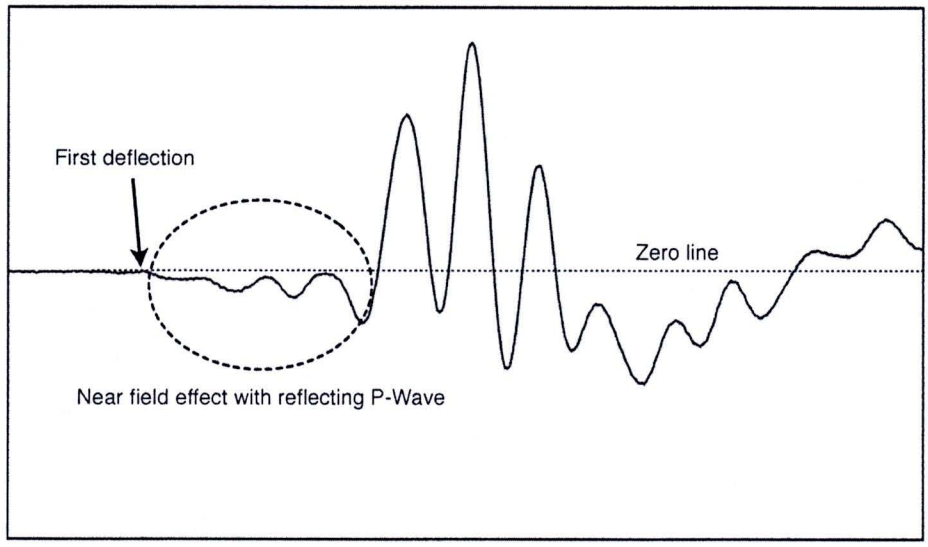

Figure 3.11 The effect of near field and reflecting *P-wave* of the receiver signal.